Electronic Supplementary Material (ESI) for Journal of Materials Chemistry C.

Supporting Information

Benign solution-processed $(Bi_xSb_{1-x})_2Se_3$ alloys for short wavelength infrared mesoporous solar cells

Jitendra Kumar, Omer Vana, Subila Kurukkal Balakrishnan, Eran Edri*

Department of Chemical Engineering, Ben-Gurion University of the Negev, Beer Sheva-8410501, Israel

Supporting information S1

Table S1. Composition ratio of $(Bi_xSb_{1-x})_2Se_3$ samples estimated from the EDS

Bi-salt molar concentration	**0.00**	**2.06**	**5.15**	**10.31**	**15.46**	**20.62**	**25.77**
$x = \frac{Bi}{(Bi+Sb)}$	0.00	0.04 ± 0.01	0.08 ± 0.02	0.11 ± 0.03	0.13 ± 0.01	0.14 ± 0.02	0.16 ± 0.01
$\frac{(S+Se)}{(Bi+Sb)}$	1.49 ± 0.06	1.46 ± 0.08	1.46 ± 0.05	1.43 ± 0.05	1.50 ± 0.07	1.48 ± 0.03	1.52 ± 0.03
$\frac{Se}{(Se+S)}$	0.88 ± 0.01	0.86 ± 0.01	0.85 ± 0.01	0.86 ± 0.02	0.92 ± 0.01	0.93 ± 0.02	0.93 ± 0.01
$\frac{Se}{(Bi+Sb)}$	1.32 ± 0.05	1.26 ± 0.06	1.24 ± 0.05	1.22 ± 0.04	1.38 ± 0.07	1.37 ± 0.03	1.40 ± 0.04
Bi-salt molar concentration	**30.92**	**41.23**	**51.54**	**61.85**	**72.15**	**82.46**	**92.77**
$x = \frac{Bi}{(Bi+Sb)}$	0.19 ± 0.04	0.23 ± 0.02	0.23 ± 0.05	0.24 ± 0.04	0.26 ± 0.04	0.29 ± 0.02	0.30 ± 0.07
$\frac{(S+Se)}{(Bi+Sb)}$	1.50 ± 0.06	1.43 ± 0.08	1.58 ± 0.05	1.54 ± 0.08	1.52 ± 0.06	1.52 ± 0.07	1.49 ± 0.04
$\frac{Se}{(Se+S)}$	0.91 ± 0.08	0.91 ± 0.02	0.82 ± 0.02	0.83 ± 0.04	0.80 ± 0.02	0.80 ± 0.01	0.77 ± 0.04
$\frac{Se}{(Bi+Sb)}$	1.37 ± 0.05	1.31 ± 0.07	1.28 ± 0.03	1.27 ± 0.09	1.21 ± 0.05	1.21 ± 0.07	1.15 ± 0.05

*for Bi-salt [$Bi(NO_3)_3 \cdot 5H_2O$] > 41.23 mM ($x > 0.23$), formation of Bi_2Se_3 secondary phase was observed in the $(Bi_xSb_{1-x})_2Se_3$ samples

Supporting information S2

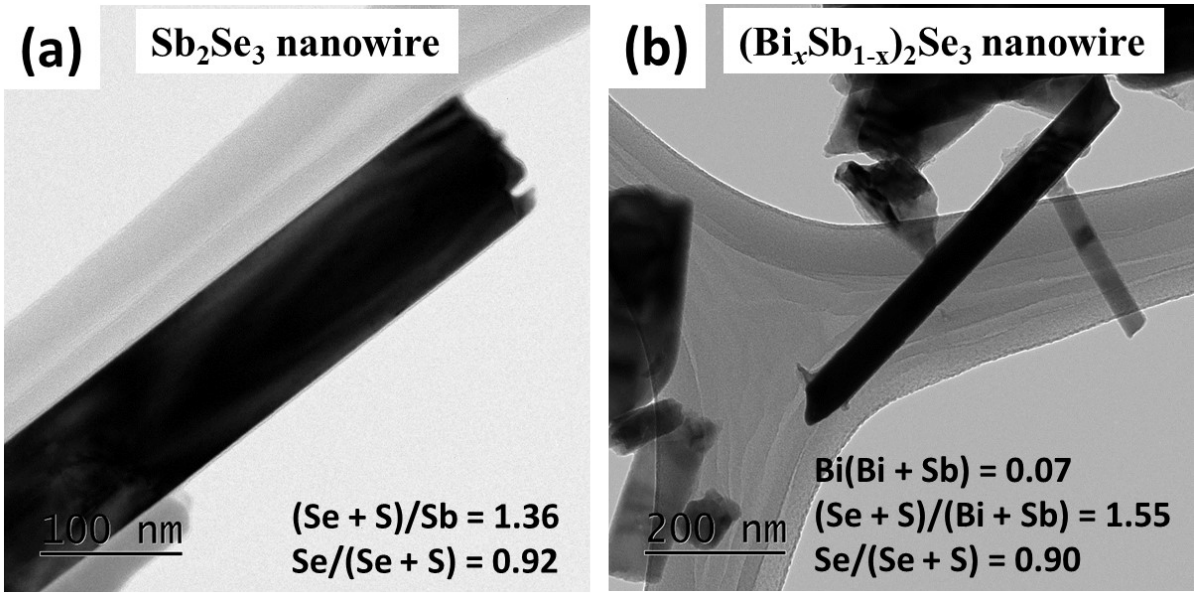

Figure S2. (a) and (b) are the TEM images of the Sb_2Se_3 and $(Bi_xSb_{1-x})_2Se_3$ nanowires, respectively. EDS composition shows that there is an incorporation of sulfur and bismuth is inside the individual nanowires.

Supporting information S3

To quantitatively understand the behaviour of the preferred orientation, the texture coefficient (TC) of the Sb_2Se_3 sample film has been calculated using equation (1)

$$TC_{hkl} = \frac{I_{hkl}}{I_{0,hkl}} \Big/ \frac{1}{N}\sum_{i=1}^{N}\frac{I_{h_i k_i l_i}}{I_{0,h_i k_i l_i}} \qquad (1)$$

Where I_{hkl} is the intensity of the diffraction peaks corresponding to hkl reflection $I_{o,hkl}$ is the intensity of hkl reflection of the standard Sb_2Se_3 (JCPDS no. 051-0861). N is the number of reflections considered for the calculation.

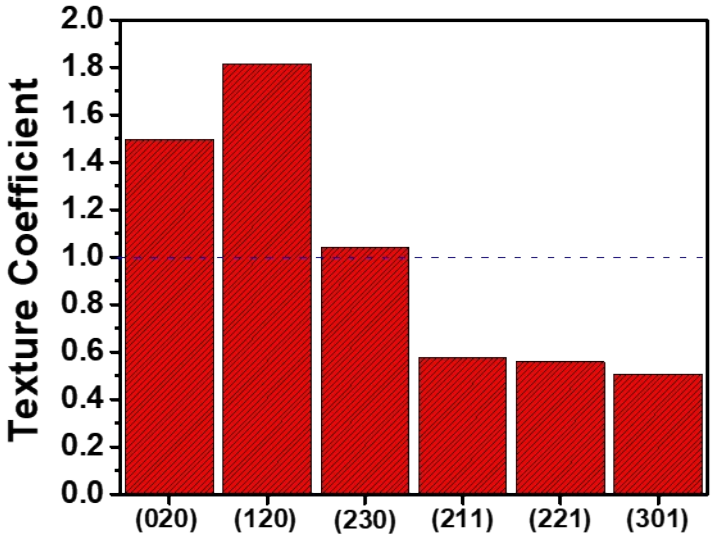

Figure S3. Texture coefficient (TC) of the Sb_2Se_3 sample estimated for (hk0) and (hk1) family of planes

Supporting information S4

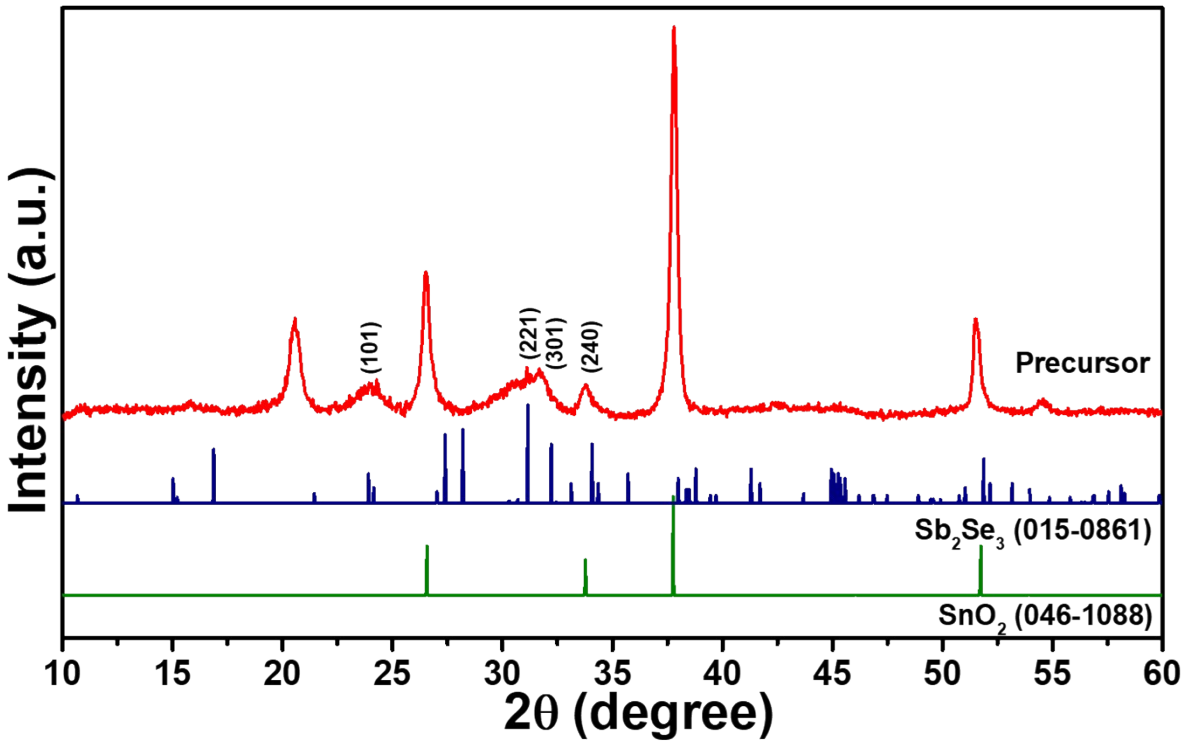

Figure S4. XRD pattern of the precursor samples deposited using the Sb-Se-ink by low-temperature heat-treatment at 100 °C for 3 min. The reference standard XRD pattern of Sb_2Se_3 (JCPDS no. 015-0861) and SnO_2 (046-1088) is also shown at the bottom of plots.

Supporting information S5

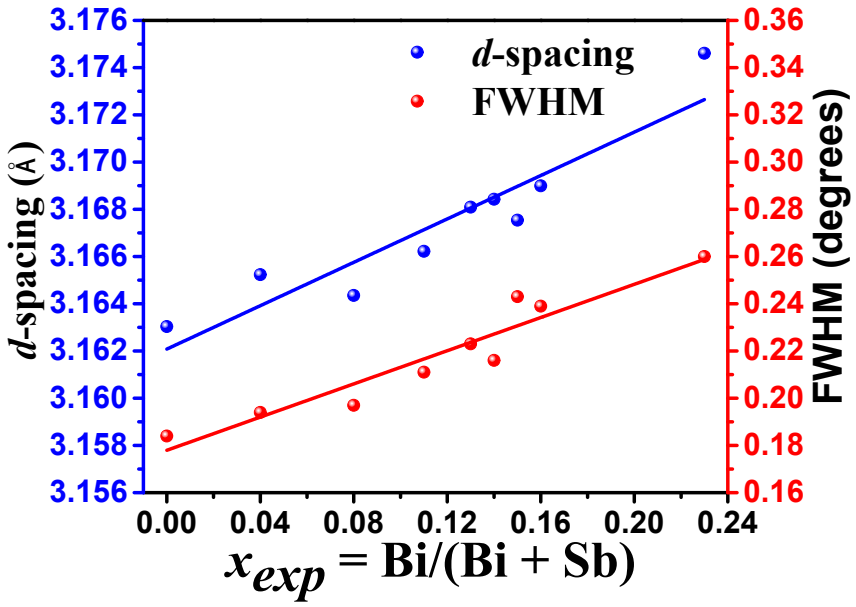

Figure S5. A plot of FWHM of X-ray diffraction peak from (221) plane at 31.13 degrees and the corresponding inter-planar spacing (*d*) for different *Bi*-content in $(Bi_xSb_{1-x})_2Se_3$ sample.

Supporting information S6

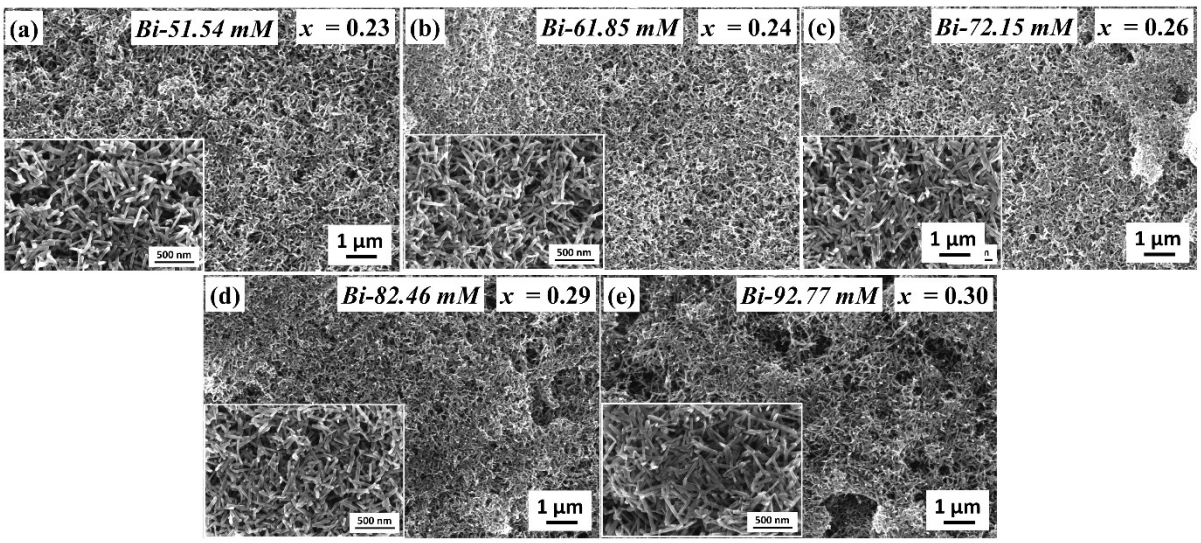

Figure S6. (a) – (e) Top view FESEM images of the $(Bi_xSb_{1-x})_2Se_3$ samples for which we detect the presence of Bi_2Se_3 secondary phase. The amount of *Bi*-salt used in Bi-stock solution and the experimentally estimated *Bi*-content [$x = Bi/(Bi + Sb)$] are also mentioned on the top side of the images. Inset is a high-resolution FESEM image for a closer view. The composition ratios of these samples are mentioned in supporting information S1.

Table S6. Nanowires diameter estimated from the FESEM micrographs

Bi-salt amount (mg)	250	300	350	400	450
Nanowire diameter (nm)	40.78 ± 8.67	34.12 ± 7.42	36.78 ± 7.51	35.24 ± 6.93	41.51 ± 9.05

The diameter for the nanowire on an average remains nearly the same for the sample for which we have observed the formation of the Bi_2Se_3 secondary phase.

Supporting information S7

The optical bandgap of the $(Bi_xSb_{1-x})_2Se_3$ thin films was estimated by measuring the diffuse reflectance on UV-Vis-NIR spectrophotometer.

Using Kubelka-Munk (KM) function the reflectance spectrum can be transformed to the corresponding absorbtion spectrum using eq. (1) [1]

(1) $$F(R) = \alpha/S = (1-R)^2/2R]$$

Using Tauc method the energy dependent absorbction coefficient (α) can be expressed by following eq. (2) [2-3]

(2) $$(\alpha h\nu)^{\frac{1}{n}} = B(h\nu - E_g)$$

Combining eq1 and eq2

(3) $$[F(R)h\nu]^{\frac{1}{n}} = B(h\nu - E_g)$$

The value of n is equal to 1/2 or 2 for the direct and indirect transition bandgaps, respectively.

The bandgaps were estimated by a linear fit of the linear part of the KM plot. Errors for the bandgaps are estimate by shifting the fitting range by ± 10 meV.

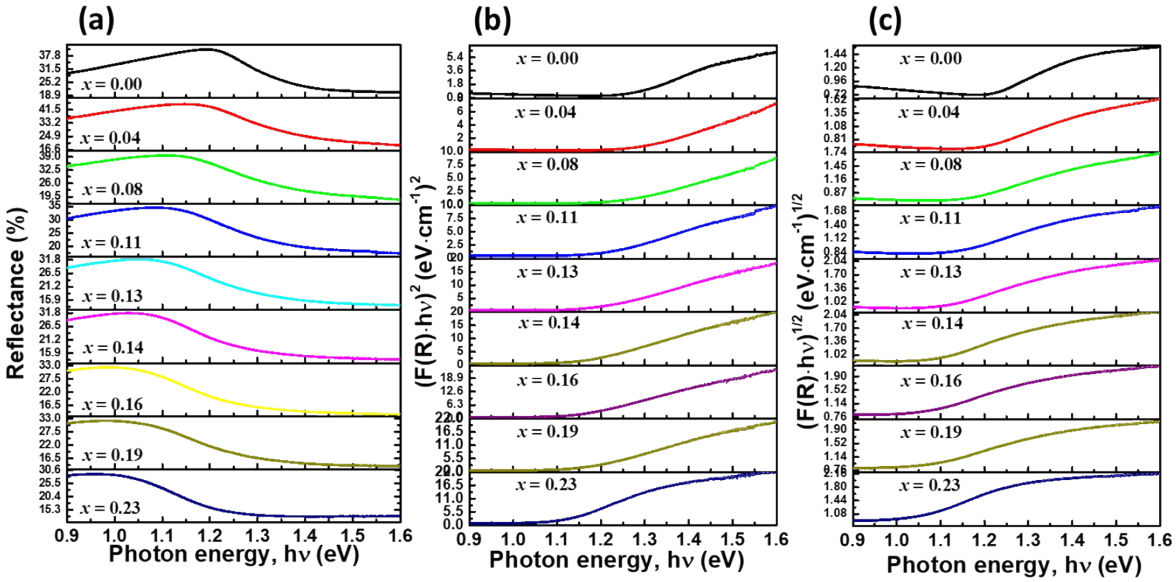

Figure S7. Reflectance and corresponding KM plot for various amount of *Bi*-content in $(Bi_xSb_{1-x})_2Se_3$ samples (b) for direct bandgap (n = ½) (c) for indirect bandgap (n = 2).

1. E.N. Davis, Developments in Applied Spectroscopy, Springer US, 1965. https://doi.org/10.1007/978-1-4684-8691-9
2. J. Tauc, R. Grigorovici, A. Vancu, Optical Properties and Electronic Structure of Amorphous Germanium, Phys. Status Solidi. 15 (1966) 627–637. https://doi.org/10.1002/pssb.19660150224.

3. N.F. Mott, E.A. Davis, Conduction in non-crystalline systems V. Conductivity, optical absorption and photoconductivity in amorphous semiconductors, Philos. Mag. 22 (1970) 903–922. https://doi.org/10.1080/14786437008221061.

Supporting information S8

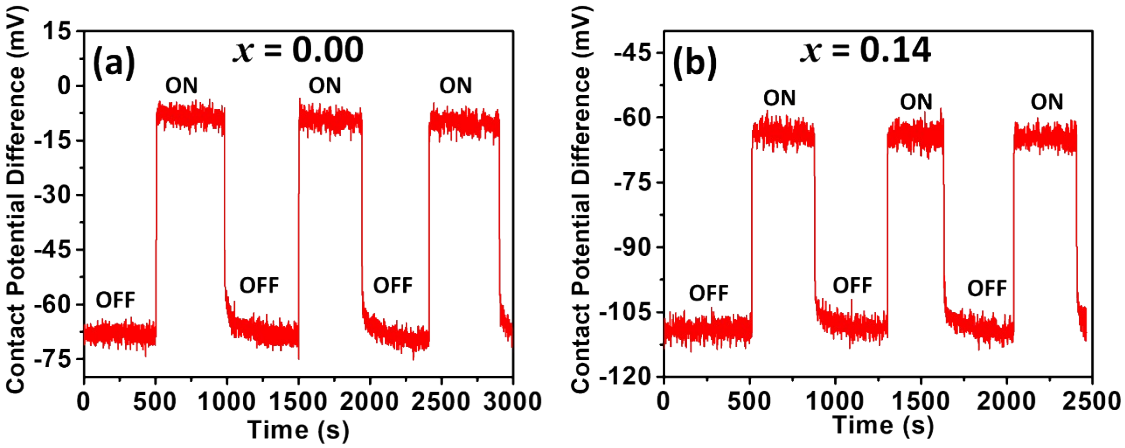

Figure S8. Surface photovoltage of Sb_2Se_3 (x = 0.00) and Bi-incorporated Sb_2Se_3 nanowires (x = 0.14) measured in dark and under the illumination of 700 nm light source. The measurement indicates the p-type behavior as both Sb_2Se_3 and Bi-incorporated Sb_2Se_3 have a positive surface voltage (SPV) value (CPD_{light} –CPD_{dark}).

Supporting information S9

Table S9-I. $(Bi_xSb_{1-x})_2Se_3$ (x = 0.00) nanowire solar cell performance parameters (*PCE* is power conversion efficiency, J_{sc} is short circuit current, *FF* is fill factor, R_{sh} is shunt resistance, R_s is series resistance). The cell with the highest *PCE* has been highlighted.

Solar cell	*PCE* (%)	*FF* (%)	J_{sc} (mA/cm²)	V_{oc} (mV)	R_{sh} (Ω·cm²)	R_s (Ω·cm²)
Cell 1	0.08	37.47	-0.67	314.27	1214.37	204.57
Cell 2	0.05	34.24	-0.55	276.08	977.87	264.24
Cell 3	0.06	32.50	-0.71	241.86	534.14	192.55
Cell 4	**0.15**	**39.59**	**-1.11**	**343.82**	**856.13**	**114.53**
Cell 5	0.02	27.99	-1.03	086.51	98.45	64.51

Table S9-II. $(Bi_xSb_{1-x})_2Se_3$ (x = 0.23) nanowire solar cell performance parameters (*PCE* is power conversion efficiency, J_{sc} is short circuit current, *FF* is fill factor, R_{sh} is shunt resistance, R_s is series resistance). The cell with the highest *PCE* has been highlighted.

Solar cell	*PCE* (%)	*FF* (%)	J_{sc} (mA/cm²)	V_{oc} (mV)	R_{sh} (Ω·cm²)	R_s (Ω·cm²)
Cell 1	0.10	34.93	-0.88	313.39	725.68	184.56
Cell 2	0.08	34.01	-0.84	293.63	652.33	186.40
Cell 3	**0.10**	**34.16**	**-0.86**	**343.30**	**742.58**	**212.77**
Cell 4	0.01	26.16	-0.41	54.51	138.50	119.73
Cell 5	0.06	33.52	-0.57	322.89	961.12	281.13

Cell 6	0.09	39.25	-0.58	379.63	1776.83	247.59
Cell 7	0.06	33.49	-0.57	316.02	985.70	292.20